Improvement of the depth resolution in depth-resolved wavenumber-scanning interferometry using multiple uncorrelated wavenumber bands

Article *in* Applied Optics · July 2013

DOI: 10.1364/AO.52.004890 · Source: PubMed

8 authors, including:

Bo Dong
Beihang University (BUAA)
19 PUBLICATIONS **32** CITATIONS
SEE PROFILE

Yulei Bai
GuangDong University of Technology
19 PUBLICATIONS **36** CITATIONS
SEE PROFILE

Cong Shi
Stevens Institute of Technology
6 PUBLICATIONS **50** CITATIONS
SEE PROFILE

Yanzhou Zhou
GuangDong University of Technology
34 PUBLICATIONS **247** CITATIONS
SEE PROFILE

Improvement of the depth resolution in depth-resolved wavenumber-scanning interferometry using multiple uncorrelated wavenumber bands

Jinxiong Xu, Yufei Liu, Bo Dong, Yulei Bai, Linlin Hu, Cong Shi, Zhuoming Xu, and Yanzhou Zhou*

Faculty of Automation, Guangdong University of Technology, Guangzhou, Guangdong 510006, China

*Corresponding author: zhouyanzhou@hotmail.com

Received 19 December 2012; revised 25 April 2013; accepted 27 April 2013; posted 10 June 2013 (Doc. ID 182111); published 5 July 2013

In this article, we provide a method to improve the depth resolution of wide-field depth-resolved wavenumber-scanning interferometry (DRWSI), because its depth resolution is limited by the range of the wavenumber scanning and mode hopping of the light source. An optical wedge is put into the optical path to measure the series of the wavenumber on time using a 2D spatial Fourier transform (FT) of the interferograms. Those uncorrelated multiple bands of the wavenumbers due to mode hopping of the diode laser can be synthesized into one band, to enlarge the range of the wavenumber scanning. A random-sampling FT is put forward to evaluate the distribution of frequencies and phases of the multiple surfaces measured. The benefit is that the depth resolution of the DRWSI is enhanced significantly with a higher signal-to-noise ratio. Because of its simplicity and practicability, this method broadens the way to employing multiple different lasers or lasers with mode hopping as the light sources in the DRWSI.

OCIS codes: (140.2020) Diode lasers; (120.3180) Interferometry; (350.5730) Resolution; (120.5050) Phase measurement; (120.6650) Surface measurements, figure.

http://dx.doi.org/10.1364/AO.52.004890

1. Introduction

Wide-field depth-resolved wavenumber-scanning interferometry (DRWSI) or swept-source optical coherence tomography (SSOCT) is a noninvasive 3D imaging technique, using wavenumber-scanning technology to detect the 3D structure and deformation field, etc., with the advantages of a large depth-resolved range and stationary components [1–5]. The technology can be traced back to digital phase-shifting interferometry using a directly frequency-modulated diode laser in the 1980s, when phase shifting was found by altering the current to tune its wavelength [6]. In 2003, Deck proposed a depth-resolved algorithm of the phase shifting to measure the microdisplacements of the multiple surfaces in stacks [7]. In 2012, Chakraborty and Ruiz proposed a configuration to use an InGaAs camera and a diode laser in the near-IR 1.3 μm range, whose wavelength can be scanned about 100 nm free of mode hopping [8]. The advantage is that this range of wavelength scanning makes the DRWSI have the finest depth resolution, at the expense of a relatively complex bulky optical system. Ruiz and Huntley *et al.* provided a solution to employ a wide-field CCD camera and an external-cavity diode laser or a Ti:sapphire laser as the laser sources [2–5] in the DRWSI. The advantage is that it makes full use of the mature technology so as to improve its performance

Due to its low cost, compact size, and multiple wavelength bands, the single-longitude-mode Fabry–Perot diode laser is a very promising application of DRWSI. Altering its temperature causes a change

1559-128X/13/204890-08$15.00/0

in the refractive index. A change in the refractive index alters the wavelength of the laser output. The only obstacle to prevent its further development is mode hopping in the output of these laser sources, which breaks the whole range of the wavelength or wavenumber scanning into uncorrelated narrow bands, and results in a poor depth resolution in the DRWSI. In 2012, Davila *et al.* described a method to record the fringe patterns of multiple optical wedges to measure the wavenumbers on time with high resolution and immunity to the ambiguities caused by large wavenumber jumps [4,5]. Furthermore, in order to overcome the nonlinearity or the mode hops of the laser, the series of unequal-space sampling is linearly fitted for the Fourier transform (FT). The method can be used to deal with mode hopping of the laser sources in the DRWSI.

In this paper, a low-cost and robust solution has been proposed to improve the depth resolution of the DRWSI dramatically. In Section 2, we introduce the optical system setup. In Section 3, we describe the measurement and algorithm to evaluate the series of wavenumbers using the spatial FT of the fringe patterns reflected from an optical wedge frame by frame. In Section 4, a random-sampling FT (RSFT) is put forward to evaluate the 3D distribution of frequencies and phases, as the wavenumber is scanned. In Section 5, the multiple uncorrelated wavenumber-scanning bands are synthesized into one band, and the experimental results show that the depth resolution of the DRWSI is improved significantly. In Section 6, we present a discussion on the disadvantages and refinement, and we provide some conclusions.

2. Optical Setup

Shown in Fig. 1(a), a Fizeau interferometer was built up and allows the DRWSI in reflection geometry. Installed on the TE-Cooled Mount TCLDM9 (Thorlabs Co), the light source was a diode laser HL7851G (Thorlabs Co) with its driving current and case temperature controlled by a diode laser controller LDC-3724C (ILX Lightwave Co). Shown in Fig. 1(b), the output of the diode laser, centered at 780 nm, could be tuned up to the maximum range of 1.38 nm with mode hops, as its case temperature was modulated from about 20°C to 40°C or from about 40°C to 20°C; at the same time, nearly 400 fringe patterns were imaged by a CCD camera (MV-VS142FM, 1392 × 1040 pixels. In the experiment, the pixel size was binned to be 696 × 520).

3. Evaluation of the Series of Wavenumbers

Shown in Fig. 1(a), the object to be measured is composed of multiple transparent surfaces $1, 2, \ldots, M$ in stacks, where 1 and 2 represent the optical wedges. The reflective light intensity forms the interferometric fringe pattern on the imaging plane of the CCD camera. If the wavenumber of the light source is scanned with time as $k(t) = 2\pi/\lambda(t)$, the fringe pattern can be denoted as [2,3,8]

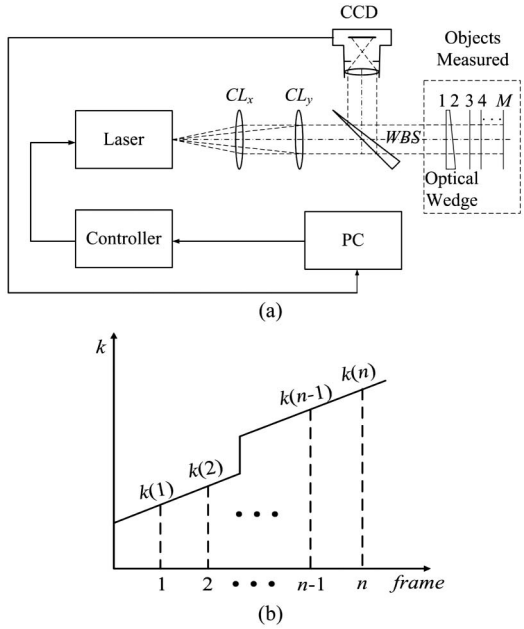

Fig. 1. Principle of DRWSI. (a) System of DRWSI. (b) Schematic of wavenumber scanning.

$$I(x,y,k) = \sum_{p=1}^{M}\sum_{q=1}^{M}\sqrt{I_p(x,y)\cdot I_q(x,y)} \times \cos\left[2\pi\cdot\frac{\Lambda_{pq}(x,y)}{\pi}\cdot k + \phi_{pq0}(x,y)\right], \quad (1)$$

where I is the reflective light intensity; x and y are the spatial coordinates of the object to be measured; the subscripts p and q represent the surfaces p and q, respectively; Λ is the difference of the optical distance; and ϕ_{pq0} is the initial interferometric phase between surfaces p and q, respectively. In Eq. (1), the cosine term is equivalent to $\cos(2\pi f k + \Phi)$; therefore $f = \Lambda/\pi$ is defined as an interferometric frequency in the k space.

When the object to be measured is an optical wedge (Glass K9, refractive index ~1.51, flatness ~$\lambda/10$) with the thinnest optical distance $\Lambda_{120} = 4.68 \pm 0.001$ mm and the title angle 12′, the fringes are straight, as shown in Fig. 2(a). The CCD camera snapped 400 fringe images, as the wavenumber of the diode laser is scanned monotonically by the modulation of the temperature. According to Eq. (1), the fringe patterns can be described as

$$I(x,y,n) = I_1 + I_2 + 2\sqrt{I_1\cdot I_2} \cdot \cos\left[2\pi\cdot\frac{\Lambda_{12}(x,y)}{\pi}\cdot k(n) + \phi_{120}(x,y)\right], \quad (2)$$

$$\Lambda_{12}(x,y) = \Lambda_{120} + \Delta\Lambda_{12x}\cdot(x-1) + \Delta\Lambda_{12y}\cdot(y-1), \quad (3)$$

where n $(n = 1, 2, \ldots, 400)$ is the index as the wavenumber is scanned, whereas $k(n)$ is its corresponding

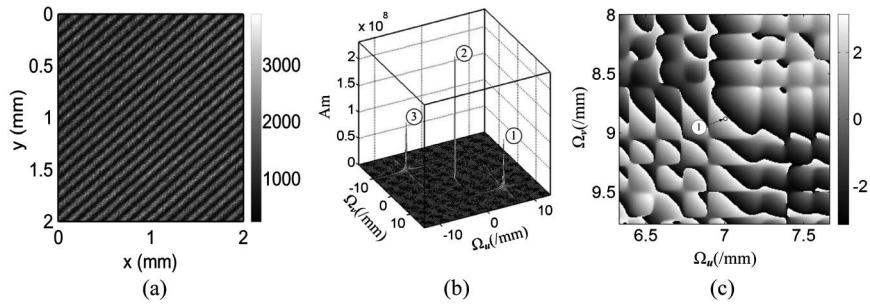

Fig. 2. Interferometry from the two smooth surfaces of the optical wedge: (a) fringe pattern, (b) map of the amplitude, where ① and ③ are the peaks of the spatial carrier frequency of the straight fringes, and ② is the DC component, and (c) map of the wrapped phase.

wavenumber, and $\Delta\Lambda_{12x}$ and $\Delta\Lambda_{12y}$ are the differences of the optical distances per pixel along the directions of x and y, respectively. Shown in Figs. 2(b) and 2(c), the 2D spatial FT of the fringe pattern frame by frame is

$$F(u,v,n) = (I_1 + I_2)\cdot\delta(u,v) + \sqrt{I_1\cdot I_2} \times \delta[u \pm \Omega_{12u}(n), v \pm \Omega_{12v}(n)] \cdot \exp[\mp j\cdot\Psi_{12}(n)], \quad (4)$$

$$\Omega_{12u}(n) = \frac{\Delta\Lambda_{12x}}{\pi}\cdot k(n)$$
$$\Omega_{12v}(n) = \frac{\Delta\Lambda_{12y}}{\pi}\cdot k(n)$$
$$\Psi_{12}(n) = 2\Lambda_{120}\cdot k(n) + \phi_{120}, \quad (5)$$

where u and v are the 2D coordinates of the spatial frequency in the directions of x and y, respectively, and $\delta(u,v)$ is the 2D delta function. Because the fringes are straight, their amplitudes Ω_{12u} and Ω_{12v} $[\Omega_{12} = (\Omega_{12u}^2 + \Omega_{12v}^2)^{1/2}]$ in the frequency-domain should be two delta functions ① and ③ symmetrical about the origin (0/mm, 0/mm, respectively. Ψ_{12} is their corresponding actual spatial phase, which is possibly more than many 2π. If the differences of the spatial frequency and the actual spatial phase between the wavenumber indices $n = a$ and $n = b$ are defined as $\Delta\Omega_{12}(a,b) = \Omega_{12}(b) - \Omega_{12}(a)$ and $\Delta\Psi_{12}(a,b) = \Psi_{12}(b) - \Psi_{12}(a)$, respectively, their ratio Γ should be constant:

$$\Gamma = \frac{\Delta\Psi_{12}(a,b)}{\Delta\Omega_{12}(a,b)} = \frac{2\pi\cdot\Lambda_{120}}{\sqrt{\Delta\Lambda_{12x}^2 + \Delta\Lambda_{12y}^2}}. \quad (6)$$

The wavenumber $k(n)$ can be expressed by the spatial frequency and the actual spatial phase, respectively:

$$k(n) = \frac{\pi\cdot\Omega_{12}(n)}{\sqrt{\Delta\Lambda_{12x}^2 + \Delta\Lambda_{12y}^2}}, \quad (7)$$

$$k(n) = \frac{\Psi_{12}(n)}{2\cdot\Lambda_{120}} - \frac{\phi_{120}}{2\cdot\Lambda_{120}}. \quad (8)$$

Equation (7) reveals that the spatial frequency can be used to evaluate the wavenumber k. Its advantage is that the linear relation between the spatial frequency and the wavenumber k is constant, no matter whether the diode laser is scanned with or without mode hopping, whereas its disadvantage is a relatively low sensitivity for the range when the spatial frequency is narrow. Figure 3(a) shows the relation between the series of wavenumbers k and its corresponding series of spatial frequencies Ω_{12}, measured from the optical wedge frame by frame, as the wavenumber of the laser is scanned. Although Eq. (8) could also be used to evaluate the wavenumber k, the phase directly deduced from the 2D spatial FT is not the actual spatial phase Ψ_{12} at all, but the wrapped spatial

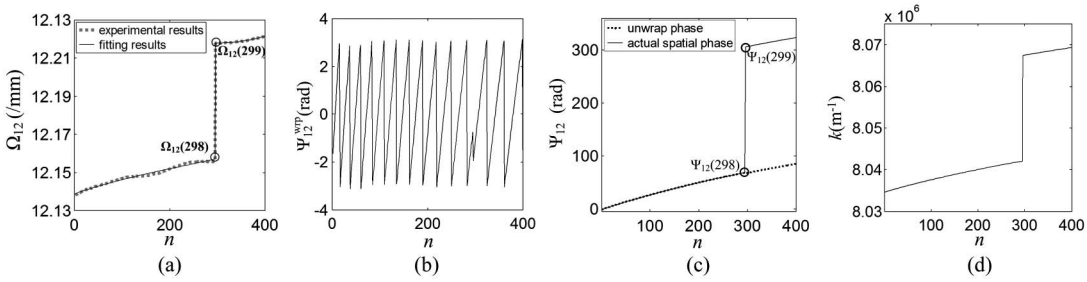

Fig. 3. Series of spatial frequencies, spatial phases, and wavenumbers. (a), (b) Series of spatial frequencies and wrapped spatial phases at the peak①, respectively. (c) Series of unwrapped spatial phases and actual spatial phases at the peak①. (d) Series of wavenumbers.

phase Ψ_{12}^{wrp}. As shown in Fig. 3(b), Ψ_{12}^{wrp} is wrapped into $[-\pi,\pi]$, due to the range of the arctan function in the 2D spatial FT being constrained to this interval. Figure 3(b) is the series of wrapped spatial phases Ψ_{12}^{wrp}, whereas $\Psi_{12}^{\mathrm{unwrp}}$ in Fig. 3(c) is the series of unwrapped phases directly unwrapped from Fig. 3(b). If the diode laser is scanned without mode hopping, the series of unwrapped spatial phases $\Psi_{12}^{\mathrm{unwrp}}$ is equal to the series of actual spatial phases Ψ_{12}, which is linearly proportional to the series of wavenumbers k with high fidelity [9]. Once the output of the diode laser has mode hopping, the difference between the adjacent actual spatial phases would be possibly more than 2π. However, because the series of unwrapped phases $\Psi_{12}^{\mathrm{unwrp}}$ cannot reflect any phase jump more than 2π, it is impossible to use $\Psi_{12}^{\mathrm{unwrp}}$ to evaluate the series of wavenumbers as mode hopping happens. Unfortunately, mode hopping exists in many laser sources, such as diode lasers, external-cavity diode lasers, Ti:sapphire lasers, etc. [2–5]. It is common in DRWSI that the depth resolution is limited by the mode hopping of the laser source.

In order to deal with the problem that the effective bandwidth of the wavenumber scanning is limited by the mode hopping of the diode laser, we propose a new method to compute the series of wavenumbers, which includes two steps:

(1) As the output of the diode laser is scanned without mode hopping, the series of unwrapped spatial phases can act as a series of actual spatial phases [9].

(2) As the output of the diode laser is scanned with mode hopping, the spatial frequency and the unwrapped spatial phase can be jointly used to evaluate the actual spatial phase. The experimental data shown in Fig. 3 are taken for example. Figure 3(a) shows the curve of spatial frequencies Ω_{12}, fitted by the third-order polynomial curve fitting function (MATLAB function "polyfit"). The advantage of the polynomial curve fitting is that the measurement error decreases $n^{1/2}$ times [10]. As the fitting of $\Omega_{12}(1)$ to $\Omega_{12}(298)$ is composed of 298 points, the error at any point is equal to 0.058 times that without fitting. The series of actual spatial phases $\Psi_{12}(1)$ to $\Psi_{12}(298)$ and $\Psi_{12}(299)$ to $\Psi_{12}(400)$ can be directly computed by 1D unwrapping, as mentioned in step (1). Γ is a constant deduced according to Eq. (6) using the average values of $\Psi_{12}(1)$ to $\Psi_{12}(298)$ and $\Omega_{12}(1)$ to $\Omega_{12}(298)$, respectively. It should be noted that a mode hop happens as the wavenumber k is being scanned from 298 to 299. According to Eq. (6), the jumping of the actual spatial phases can be calculated by $\Delta\Psi_{12}(298,299) = \Gamma * \Delta\Omega_{12}(298,299)$. The actual spatial phase can therefore be computed as $\Psi_{12}(299) = \Psi_{12}(298) + \Gamma * \Delta\Omega_{12}(298,299)$, where $\Delta\Omega_{12}(298,299)$ is the difference of the spatial frequencies between 298 and 299 after being fitted by the spine function. In the end, the whole series of the actual spatial phase is shown in Fig. 3(c). The series of wavenumbers deduced according to Eq. (8), using Ω_{12}, ϕ_{120}, and Λ_{120}, is shown in Fig. 3(d).

In the practical application, the object to be measured is composed of multiple transparent surfaces $1,2,3,\ldots,M$. The fringe patterns are transformed spatially to the frequency domain frame by frame. We can carefully design the optical distance between the two surfaces of the optical wedge, and the optical distance between the optical wedge and the other multiple surfaces measured to evade their spectrum mixing. As shown in Figs. 2(b) and 2(c), at the position of the peak ① in the spatial spectrum of every fringe pattern, the series of actual spatial phases and the series of wavenumbers are evaluated according to the method above. In the following sections, the series of wavenumbers is used to decompose the maps of the frequencies and phases of the multiple surfaces using the RSFT.

4. Random-Sampling Fourier Transform

As the wavenumber of the diode laser is scanned, it is often accompanied by nonlinearity and mode hopping. Due to the traditional FT being based on equally spaced sampling, nonlinear or random sampling would generally lead to a large spectral error in the spectrum evaluation. Therefore, a new algorithm is proposed to solve this problem in the following. The FT of the sampled interferometric signal $I(x,y,k)$ can be written as

$$\begin{aligned}\tilde{I}(x,y,f) &= F[I(x,y,k)] \otimes F[w(k)] \otimes F\left[\sum_{n=1}^{N}\delta(k-k(n))\right] \\ &= \int_{-\infty}^{+\infty} I(x,y,k)\cdot w(k)\cdot\sum_{n=1}^{N}\delta(k-k(n)) \\ &\quad\cdot\exp(-j\cdot 2\pi\cdot f\cdot k)\cdot \mathrm{d}k, \end{aligned} \tag{9}$$

where $w(k)$ and $\sum_{n=1}^{N}\delta(k-k(n))$ are the window function (such as the rectangular and the hanning window functions) and the sampling function, respectively; F denotes the FT; $\otimes$ represents convolution; $k(n)$ is the value of the wavenumber as the CCD camera takes the nth image; and f is the frequency in the Fourier space k.

According to the linearity of the FT, Eq. (9) can be written as

$$\begin{aligned}\tilde{I}(x,y,f) &= \sum_{n=1}^{N}\int_{-\infty}^{+\infty}\delta[k-k(n)]\cdot I(x,y,k)\cdot w(k) \\ &\quad\cdot\exp(-j\cdot 2\pi\cdot f\cdot k)\cdot \mathrm{d}k. \end{aligned} \tag{10}$$

Due to the Dirac function having the property

$$\int_a^b \delta(k-k_0)\cdot f(k)\cdot \mathrm{d}k = f(k_0) \qquad (a<k_0<b), \tag{11}$$

Eq. (10) can be written as

$$\tilde{I}(x,y,f) = \sum_{n=1}^{N} I(x,y,k(n)) \cdot w(k(n)) \cdot \exp(-j \cdot 2\pi \cdot f \cdot k(n)). \quad (12)$$

Substituting Eq. (8) into Eq. (12), we have

$$\tilde{I}(x,y,f) = \sum_{n=1}^{N} I(x,y,k(n)) \cdot w(k(n)) \cdot \exp\left[-j \cdot 2\pi f \cdot \left(\frac{\Psi_{12}(n)}{2 \cdot \Lambda_{120}} - \frac{\phi_{120}}{2 \cdot \Lambda_{120}}\right)\right]. \quad (13)$$

In Eq. (13), the phase term $2\pi f$ $(\Phi_{120}/2\Lambda_{120})$, which has no influence on the amplitude, is proportional to the frequency with the ratio determined by the system geometry only. In Eq. (13), the spectrum of the interferometric light intensity is independent of how the series of the actual spatial phase $\Psi_{12}(n)$ is sampled and ranked; therefore, Eq. (13) is called RSFT. As the signal is sampled nonlinearly and randomly, the advantage of RSFT is that its spectrum is almost equal to the true spectrum of the original signal, while the spectrum of the traditional FT has severe distortion.

The depth resolution of the RSFT in DRWSI is [2,3]

$$\delta\Lambda = \gamma \cdot \frac{4\pi \cdot \Lambda_{120}}{\Delta\Psi_{12}(1,N)}, \quad (14)$$

where γ is the coefficient of the window function, for the rectangular window $\gamma = 1$.

As the wavenumber of the laser is scanned with the mode-hopping $s = 1, \ldots, S$, the depth range of the DRWSI is

$$\Delta\Lambda = \frac{N \cdot \pi}{2 \cdot \left(\Delta k - \sum_{s=1}^{S} \Delta k_s\right)}, \quad (15)$$

where N is the total number of fringe patterns, and Δk is the tuning range of the wavenumber. Δk_s is the difference of the wavenumbers before and after the mode-hopping $s = 1, \ldots, S$, respectively. As shown in Fig. 4(a), if the interferometric intensity is simulated as $\Delta k = 5.162 \times 10^3$ m^{-1}, $\Delta k_1 = 1.045 \times 10^3$ m^{-1}, and the total number of the sampling $N = 400$ and $I(k) = 1/2 + \cos[2\pi(\Lambda/\pi)k + 0.2]$, according to Eq. (15), the range of the depth is $\Delta\Lambda = 152.0$ mm . If we set the optical distance $\Lambda = 145$ mm and $\Lambda < \Delta\Lambda$, the interferometric intensity is shown in Fig. 4(b), with respect to the wavenumber and the index of the wavenumber scanning, respectively. Shown in Fig. 4(c), the peak in the amplitude spectrum of RSFT is located at optical path difference (OPD) = 145 mm with the amplitude 0.484, which conforms with the preset Λ. If we set the optical distance $\Lambda = 160$ mm and $\Lambda > \Delta\Lambda$, as shown in Fig. 4(d), the peak in the amplitude of RSFT

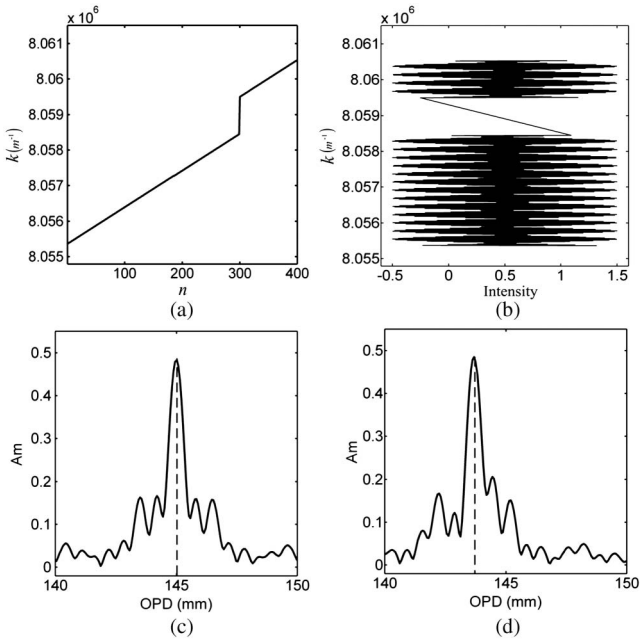

Fig. 4. Simulation of the depth range of the DRWSI. (a) Series of the wavenumber scanning where there is mode hopping. (b) Corresponding series of interferometric intensities. (c) The OPD measured is less than the range of the depth resolution. (d) The OPD measured is more than the range of the depth resolution.

is located at OPD = 143.7 mm with the amplitude 0.486, which is far from the preset Λ. The error of the latter is caused by the signal frequency greater than the sampling rate.

In order to verify the effectiveness of RSFT, the object to be measured is composed of three optical smooth surfaces with the optical distances $\Lambda_{12} = 4.68 \pm 0.001$ mm and $\Lambda_{23} = 17.18 \pm 0.05$ mm, respectively. 1 and 2 represent the optical wedges. As the range of the wavenumber $\Delta k = 3.89 \times 10^3$ m^{-1} without mode hopping, the series of wavenumbers is measured on time, as shown in Fig. 5(a). The series of reflective interferometric light intensities in ($x = 0$ mm, $y = 0.0865$ mm) is shown in Fig. 5(b). After the DC component is removed and transformed by the RSFT with a rectangular window, the FT with a rectangular window, and the hanning window, respectively, their normalized amplitudes are shown in Fig. 5(c). The interferometric peak of Λ_{12} from the optical wedge separates far from the others and can be clearly distinguished. Its locations are at $\Lambda_{12} = 4.59$ mm transformed by the FT with the hanning window, and $\Lambda_{12} = 4.69$ mm transformed by RSFT with the rectangular window, respectively. The latter one is more accurate. The interferometric peaks of Λ_{23} and Λ_{13} transformed by the FT with the rectangular window are mixed up so that it is difficult to distinguish them. The peaks, located at $\Lambda_{23} = 16.66$ mm and $\Lambda_{13} = 21.01$ mm, respectively, transformed by the FT with the hanning window, can be distinguished, at the expense that their mainlobes are widened twice. The maximum error of the OPD at $\Lambda_{12,}$, Λ_{23}, or Λ_{13}, transformed

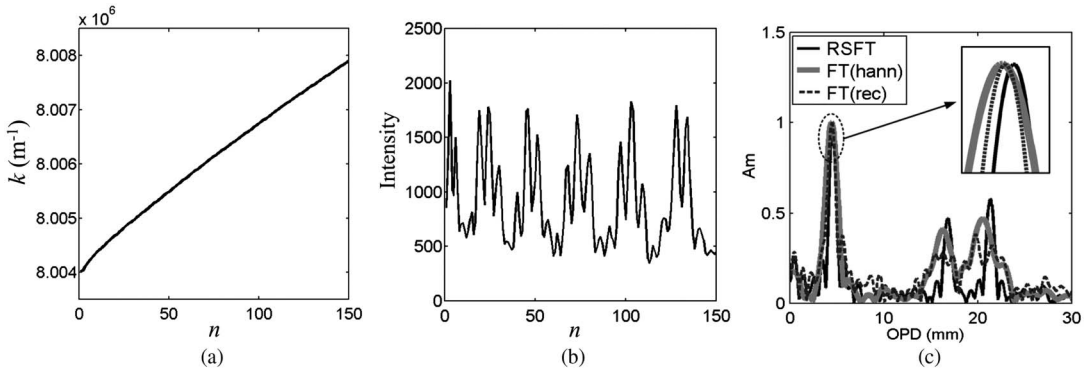

Fig. 5. RSFT in the DRWSI. (a) Series of wavenumbers measured from the optical wedge frame by frame, as the diode laser is scanned without mode hopping. (b) Series of interferometric intensities in ($x = 0$ mm, $y = 0.0865$ mm). (c) Its amplitude spectrum using the RSFT with a rectangular window, the FT with a rectangular window, and the hanning window, respectively, where all the amplitudes are normalized by their own peaks at OPD $= \Lambda_{12}$.

by the FT with the hanning window, is −0.85 mm. It should be noted that $\Lambda_{13} - \Lambda_{12} - \Lambda_{23}$ should be zero in theory; however, transformed by the FT with the hanning window, $\Lambda_{13} - \Lambda_{12} - \Lambda_{23}$ is −0.24 mm. Among the three methods, those peaks, located at $\Lambda_{23} = 17.20$ mm and $\Lambda_{13} = 21.91$ mm, transformed by the RSFT with the rectangular window, can clearly be distinguished with the highest signal-to-noise ratio, and the narrowest mainlobe. The maximum error of OPD at Λ_{12}, Λ_{23}, or Λ_{13}, transformed by the RSFT with the rectangular window, is 0.05 mm, and $\Lambda_{13} - \Lambda_{12} - \Lambda_{23}$ is 0.02 mm. Because the error of the RSFT with the rectangular window is much smaller than the error of the FT with the hanning window, the correctness of the RSFT in DRWSI is proved. In DRWSI, all of the performances of the RSFT with the rectangular window are the best among the three methods.

5. Synthesis of Multiple Uncorrelated Bands of Wavenumbers

In order to verify that the RSFT can be applied to DRWSI with mode hopping, the object to be measured is changed to be four smooth flat surfaces. 1 and 2 represent the optical wedges used in the previous section, whereas 3 and 4 represent a flat glass plate $\Lambda_{34} = 7.43 \pm 0.05$ mm. The optical distance between 2 and 3 is the air gap with $\Lambda_{23} = 0.5 \pm 0.05$ mm. Since the diode laser is modulated by temperature and electronic current, respectively, its wavenumber is scanned four times, as shown in Fig. 6(a). The corresponding ranges of the wavenumber scanning are 1, $\Delta k = 5.87 \times 10^3$ m^{-1}; 2, before the mode hop $\Delta k = 2.90 \times 10^3$ m^{-1}, and after the mode hop $\Delta k = 0.80 \times 10^3$ m^{-1}; 3, $\Delta k = 5.77 \times 10^3$ m^{-1}; 4, before the mode hop $\Delta k = 2.17 \times 10^3$ m^{-1}, and after the mode hop $\Delta k = 1.09 \times 10^3$ m^{-1}. The way to synthesize the four wavenumber-scanning bands into one band includes two steps: (1) all of the wavenumbers are put together, and sorted in ascending order, as shown in Fig. 6(b); (2) the interferometric light intensities are rearranged in the corresponding order of the new wavenumber series. In the end, the new series of wavenumbers and its corresponding series of light intensities form the new synthesis band of the wavenumber scanning. Because the range of wavenumber scanning is $\Delta k = 14.42 \times 10^3$ m^{-1}, and $\Delta k_1 = 4.20 \times 10^3$ m^{-1}, according to Eq. (15), the range of the depth of DRWSI is $\Delta\Lambda = 156.5$ mm. The OPDs between the surfaces measured are far lower than the range of the depth of DRWSI.

In order to show the performance of the synthesis-band DRWSI, the transection lines at $x = 0.6$ mm in Figs. 7(c) and 7(f) are taken for example. The maps of the amplitudes and phases of the single-band DRWSI 1 and the synthesis-band DRWSI are shown in Figs. 7(c)–7(h). Because the shortest optical distance Λ_{23} is the air gap 0.5 mm, and the range of any single wavenumber band 1–4 is not large enough to visualize the air gap, the peaks of Λ_{12} and Λ_{13}, Λ_{34}, and Λ_{24} in the amplitude spectrum appear to have severe spectral mixing up, as shown in Figs. 7(c) and 7(d). Using the method given above, these four wavenumber-scanning bands are synthesized to be

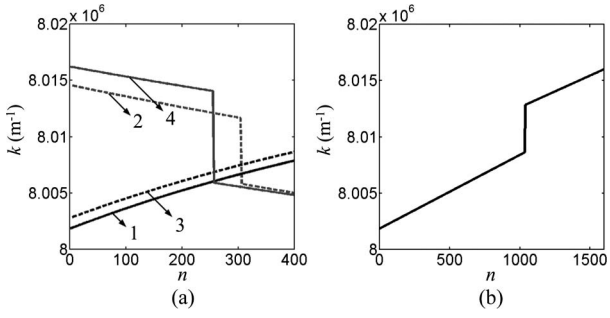

Fig. 6. Series of the wavenumbers, as the diode laser is modulated by the temperature and the current, respectively; (a) 1: the temperature from 41°C to 32°C, the driving current 135 mA; 2: the temperature from 28°C to 38°C, the driving current 135 mA; 3: the temperature from 40°C to 31°C, the driving current 115 mA; 4: the temperature from 26°C to 36°C, the driving current 115 mA and (b) the synthesis series of the multiple uncorrelated bands of the wavenumbers.

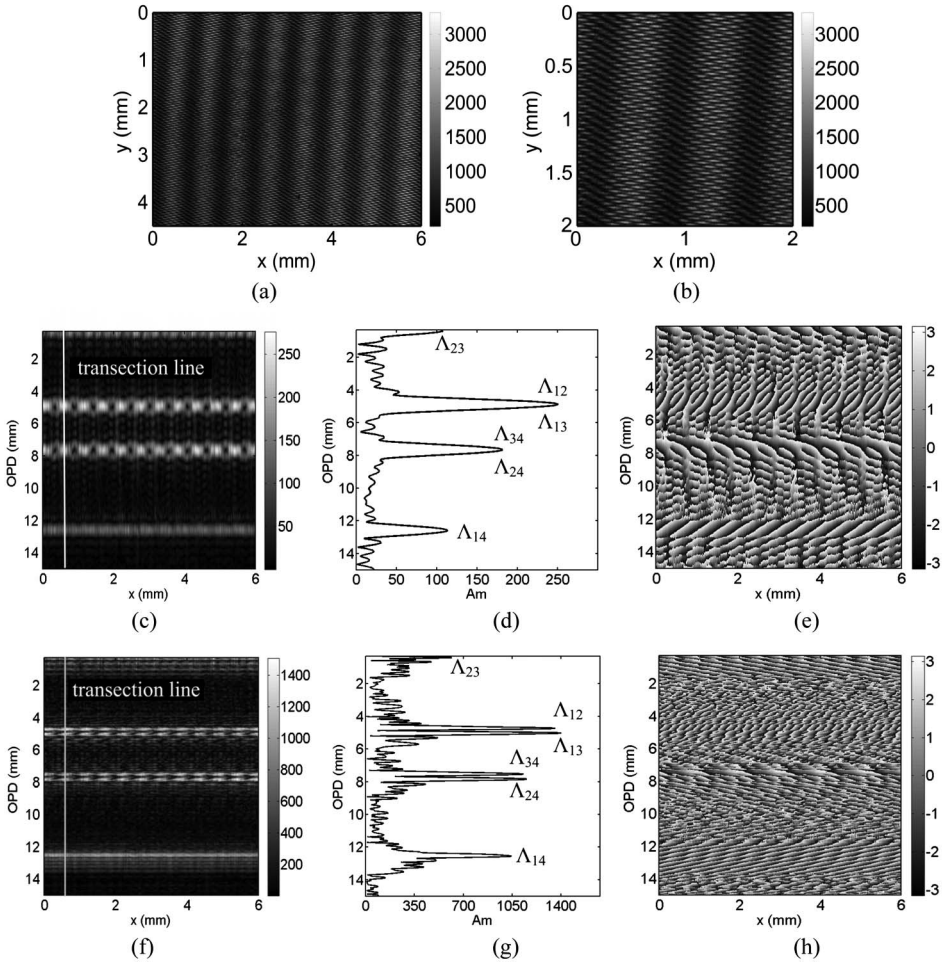

Fig. 7. Single-band and synthesis-band DRWSI. (a), (b) Fringe pattern and its zoom. (c)–(e) Maps of the amplitudes and the phases of the single-band DRWSI; the series of wavenumbers is 1 in Fig. 6(a). (f)–(h) Maps of the amplitudes and the phases of the synthesis-band DRWSI.

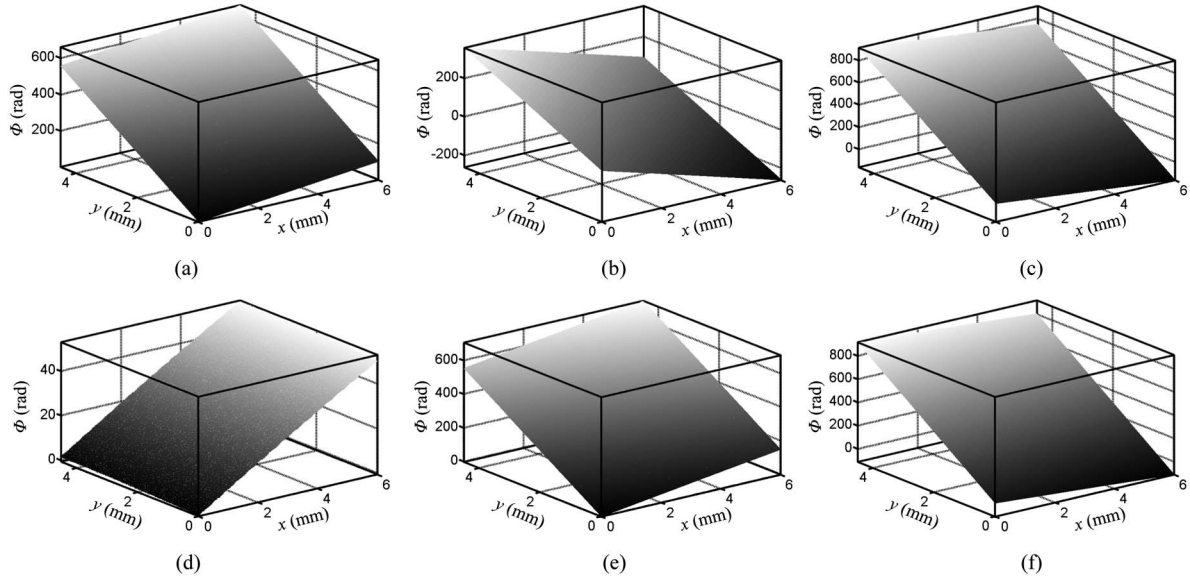

Fig. 8. Unwrapped phase maps of the smooth surfaces measured, evaluated by the synthesis-band DRWSI: (a) Λ_{23}, (b) Λ_{12}, (c) Λ_{13}, (d) Λ_{34}, (e) Λ_{24}, and (f) Λ_{14}.

one band with the range up to $\Delta k = 14.42 \times 10^3$ m^{-1} (1.38 nm), as shown in Fig. 6(b). According to Eq. (14), the depth resolution of DRWSI by the RSFT with the rectangular window is 0.44 mm. Therefore, using this synthesis wavenumber-scanning band, the peaks $\Lambda_{23} = 0.44$ mm, $\Lambda_{12} = 4.70$ mm, $\Lambda_{13} = 5.11$ mm, and $\Lambda_{34} = 7.49$ mm, $\Lambda_{24} = 7.92$ mm, $\Lambda_{14} = 12.54$ mm can be distinguished with high accuracy and fidelity, as shown in Figs. 7(f) and 7(g). Furthermore, $\Lambda_{14}-\Lambda_{12}-\Lambda_{24} = -0.08$ mm and $\Lambda_{14}-\Lambda_{13}-\Lambda_{34} = -0.06$ mm prove the correctness of the experiment. As shown in Fig. 7(e), at the positions of the spectral mixing up in the single-band DRWSI, the distribution of the phase is relatively wide and smooth, meaning the phase differences between the peaks Λ_{12} and Λ_{13}, Λ_{34} and Λ_{24} disappear. As shown in Fig. 7(h), at the corresponding positions in the synthesis-band DRWSI, the distribution of the phase is relatively narrow and varies wildly, and the phase differences between peaks Λ_{12}, Λ_{34}, and Λ_{24} appear clearly. As shown in the mesh plots of Figs. 8(a)–8(f), all the unwrapped spatial maps at the peaks Λ_{23}, Λ_{12}, Λ_{13}, Λ_{34}, Λ_{24}, and Λ_{14} represent the optical differences between the smooth flat surfaces, which conform with the preset of the object to be measured.

6. Discussion and Conclusions

Nonlinearity and mode hopping of the coherent light sources are barriers to the improvement of the depth resolution of DRWSI. In this paper, we proposed a solution to deal with this problem. First of all, an optical wedge is put into the optical path in series. It induces straight interferometric fringes at the specific band of the spatial frequency determined by the geometry of the optical wedge itself. The peak frequency and phase within this band are measured and computed frame by frame as the wavenumber of the light source is scanned by temperature. Second, these spatial frequencies and phases of the optical wedge are jointly used to compute the wavenumber series, and these multiple uncorrelated wavenumber-scanning bands are integrated into one. Third, an RSFT to evaluate the maps of the frequencies and the wrapped phases of the smooth surfaces measured is proposed to deal with the random-sampling problem of the wavenumber series. The experimental results show that the depth resolution of the DRWSI is improved from about 1.07 to 0.44 mm. Since the multiple wavenumber-scanning bands in our experiment are uncorrelated, in principle, the technology could be extended to the DRWSI, integrating many different light sources—in particular, different diode lasers. In conclusion, the synthetic-band DRWSI is practical, and likely to have a broad impact on a wide range of applications of the DRWSI

The main disadvantages of this method are (1) the speed of the wavenumber scanning is relatively slow, about 80 s/400 frames, as it is performed by temperature modulation; (2) if the mode hops are over 10% of the total range of the wavenumber scanning, parts of those small sidelobes in the amplitude spectrum become high and sharp. In some extreme cases, they are as high as those peaks from the interferometric surfaces. The details will be explored further in our future paper.

The authors thank the National Natural Science Foundation of China (NSFC) for their financial support with grant 11072063 and the Provincial Natural Science Foundation of Guangdong (NSFG) for their financial support with grant S2012010010327. We are also very appreciative of the comments from reviewer2.

References

1. M. Zysk, F. T. Nguyen, A. L. Oldenburg, D. L. Marks, and S. A. Boppart, "Tomography: a review of clinical development from bench to bedside," J. Biomed. Opt. **12**, 051403 (2007).
2. P. D. Ruiz, Y. Zhou, J. M. Huntley, and R. D. Wildman, "Depth-resolved whole-field displacement measurement using wavelength scanning interferometry," Pure Appl. Opt. **6**, 679–683 (2004).
3. P. D. Ruiz, J. M. Huntley, and R. D. Wildman, "Depth-resolved whole-field displacement measurement by wavelength-scanning electronic speckle pattern interferometry," Appl. Opt. **44**, 3945–3953 (2005).
4. A. Davila, J. M. Huntley, C. Pallikarakis, P. D. Ruiz, and J. M. Coupland, "Simultaneous wavenumber measurement and coherence detection using temporal phase unwrapping," Appl. Opt. **51**, 558–567 (2012).
5. A. Davila, J. M. Huntley, C. Pallikarakis, P. D. Ruiz, and J. M. Coupland, "Wavelength scanning interferometry using a Ti:Sapphire laser with wide tuning range," Opt. Lasers Eng. **50**, 1089–1096 (2012).
6. Y. Ishii, J. Chen, and K. Murata, "Digital phase-measuring interferometry with a tunable laser diode," Opt. Lett. **12**, 233–235 (1987).
7. L. L. Deck, "Fourier-transform phase-shifting interferometry," Appl. Opt. **42**, 2354–2365 (2003).
8. S. Chakraborty and P. D. Ruiz, "Measurement of all orthogonal components of displacement in the volume of scattering materials using wavelength scanning interferometry," J. Opt. Soc. Am. A, **29**, 1776–1785 (2012).
9. Y. J. Shen and J. M. Huntley, "Simple method to calibrate phase modulators for use in dynamic phase-shifting interferometry," Opt. Eng. **43**, 2998–3002 (2004).
10. D. C. Harris, *Quantitive Chemical Analysis*, 6th ed. (W. H. Freeman & Company, 2003).